

# UPose3D: Uncertainty-Aware 3D Human Pose Estimation with Cross-View and Temporal Cues

Vandad Davoodnia, Saeed Ghorbani, Marc-André Carbonneau, Alexandre Messier, and Ali Etemad

**Abstract**—We introduce UPose3D, a novel approach for multi-view 3D human pose estimation, addressing challenges in accuracy and scalability. Our method advances existing pose estimation frameworks by improving robustness and flexibility without requiring direct 3D annotations. At the core of our method, a pose compiler module refines predictions from a 2D keypoints estimator that operates on a single image by leveraging temporal and cross-view information. Our novel cross-view fusion strategy is scalable to any number of cameras, while our synthetic data generation strategy ensures generalization across diverse actors, scenes, and viewpoints. Finally, UPose3D leverages the prediction uncertainty of both the 2D keypoint estimator and the pose compiler module. This provides robustness to outliers and noisy data, resulting in state-of-the-art performance in out-of-distribution settings. In addition, for in-distribution settings, UPose3D yields a performance rivaling methods that rely on 3D annotated data, while being the state-of-the-art among methods relying only on 2D supervision.

**Index Terms**—Markerless Motion Capture, Multi-view Human Pose Estimation, Uncertainty Modeling, Synthetic Training

## I. INTRODUCTION

Multi-view 3D human pose estimation is a challenging task in computer vision that involves determining the 3D position of human body landmarks given videos or images from multiple synchronized cameras [1]–[3]. Compared to monocular setups, multi-view pose estimation leverages information from different viewpoints, alleviating the single-camera ambiguity and improving accuracy in challenging situations. This robustness is crucial in precision-demanding applications like markerless motion capture, essential to industries such as video gaming and filmmaking, where sub-centimeter accuracy is often required.

The conventional 3D keypoint estimation process involves two stages. Firstly, 2D landmarks are extracted from each camera view. This is followed by triangulation using the known camera parameters to infer 3D points [2], [4]. However, the accuracy of such methods heavily relies on the precision of independent 2D predictions across

views, which is problematic in scenarios with complex body-part interactions or severe occlusions. Outlier mitigation techniques such as RANdom-SAMple Consensus (RANSAC) [5] and refinement algorithms [1] offer some robustness but cannot fully address these inherent limitations. Recent advances in deep learning models that use cross-view fusion strategies [3], [6], [7] have yielded promising 3D pose estimation results. For instance, epipolar transformers [3] show the benefits of leveraging cross-view information using epipolar geometry. However, the scalability of such approaches is often hindered with additional cameras, requiring advanced techniques to maximize the agreement between several model outputs [7]. Another research direction aims to leverage rich temporal information [6], [8] to enhance pose estimation accuracy. For instance, numerous works show the impact of using large temporal context for monocular 3D pose estimation [9], [10]. Similarly, methods like MFT-Transformers [6], focusing on multi-view fusion and temporal modelings, can yield improvements over single-frame methods. However, such approaches require access to large annotated 3D datasets (multi-view video streams and corresponding 3D pose coordinates) during training, which is especially scarce in outdoor and in-the-wild settings. Furthermore, these models are often trained on limited pose and camera variations, hindering their generalization to novel views.

To address the challenges of viewpoint scalability and reliance on 3D annotated training data, we introduce UPose3D, a new method for 3D human pose refinement. Our method leverages 2D keypoints and their uncertainties from two sources to improve robustness to outliers and noisy data. These sources include: *a*) direct 2D pose estimation from RGB images, and *b*) a pose compiler module that utilizes consistency across views and over time. Additionally, we introduce a new cross-view fusion strategy to ensure scalability to different numbers of cameras before our pose compiler. Specifically, we project the keypoints from all available views onto a reference view to obtain a 2D point cloud for each joint. These are then fed to a point cloud transformer module to learn cross-view representations. These features are then passed to a spatiotemporal encoder to efficiently process temporal and skeleton information from temporal windows. To train our pose compiler without relying on 3D annotated datasets, we generate synthetic data simulating realistic multi-view human pose recordings from a large-scale motion capture dataset. This approach promotes generalization across diverse camera configurations and postures, overcoming the limitations of real-world, multi-view 3D annotated

This work was performed during an internship at Ubisoft Laforge partially funded by Mitacs through the Accelerate program.

V. Davoodnia and A. Etemad were with the Department of Electrical and Computer Engineering, Queen’s University, Kingston, Ontario, Canada. e-mail: {vandad.davoodnia,ali.etemad}@queensu.ca

V. Davoodnia and S. Ghorbani were with Ubisoft LaForge, Toronto, Ontario, Canada. e-mail: saeed.ghorbani@ubisoft.com

M. A. Carbonneau and A. Messier were with Ubisoft LaForge, Montreal, Québec, Canada. e-mail: {marc-andre.carbonneau2,alexandre.messier}@ubisoft.com

datasets.

To evaluate the performance of our proposed model, we use four widely used public datasets, Human3.6m [11], Rich [12], AMASS [13], and COCO-WholeBody [14], [15], across two separate experiment setups. More specifically, we assess the performance of our method in both in-distribution and out-of-distribution (OoD) settings to better evaluate generalizability to new environments and multi-view camera setups. These experiments demonstrate that our approach outperforms prior state-of-the-art solutions in OoD while achieving competitive performance in in-distribution settings. Next, we provide detailed ablation experiments demonstrating the impact of uncertainty modeling and our pose compiler in improving multi-view pose estimation robustness to outliers. Finally, we perform several experiments to showcase the impact of the number of camera views and larger time windows. In summary, our method achieves a high level of view-point flexibility and robustness without requiring direct 3D annotations.

Our contributions can be summarized as follows:

- We present UPose3D, a 3D human pose estimation pipeline for multi-view setups that achieves state-of-the-art results in OoD settings and performs competitively in in-distribution evaluations.
- Our method uses a novel uncertainty-aware 3D pose estimation algorithm that uses normalizing flows to leverage 2D pose distribution modeling. Experiments demonstrate that this approach is more effective than prior works using heatmaps.
- We propose a new training strategy that relies only on synthetic multi-view motion sequences generated online from motion capture data, which allows our pipeline to scale to various camera and skeleton configurations.

## II. RELATED WORKS

**3D Pose Estimation.** Traditionally triangulation techniques like RANSAC have been used for 3D human pose estimation [2], [4]. However, these methods are generally not directly differentiable and their integration into deep learning pipelines is hindered. Therefore, recent research has explored more flexible, soft-predictive models, such as volumetric 3D keypoint representations [2] and cross-view feature fusion strategies [7]. Another approach [16] introduces a stochastic framework for human pose triangulation that relies on 3D pose hypothesis generation, scoring, and selection from 2D detection of several camera views. However, the accuracy of 2D pose detectors limits most such approaches. As a result, some methods incorporate epipolar geometry for pose consistency via self-supervised [17] and semi-supervised [18] learning. More advanced techniques have explored feature fusion strategies using epipolar lines across camera pairs [3], [4], showing significant improvements. However, these methods require complex re-projection in view pairs, limiting their scalability to any number of cameras or different camera placements due to the lack of camera variety in the training set.

To avoid the reliance on large number of parameters, a recent work [6] proposed a multi-view and temporal transformer network to perform an end-to-end 3D pose estimation without relying on camera parameters via leveraging cross-view feature fusion. Other works have conducted experiments on using human pose priors using generative models such as GANs [19] and Diffusion probabilistic models [20] to perform 3D pose estimations from a variety of inputs. However, most such approaches rely on 3D pose annotations from in-studio collected datasets to train their model.

Another research track explores the benefits of uncertainty modeling for 3D human pose estimation for enhancing the performance in occlusion-heavy scenarios [21], [22]. For example, Residual Log-likelihood Estimation (RLE) [23], has been proposed to model the underlying distribution of 2D keypoints in human pose estimation via regression. This approach leverages a re-parameterization technique and normalizing flows to learn keypoint uncertainty and achieves similar performance to heatmap-based [24], [25] and SimCC-based [26] techniques. One advantage of such uncertainty modeling techniques that we exploit in this paper is their ability to estimate the likelihood of keypoints in an image in a differentiable process, which other methods lack.

**Transformers in Pose Estimation.** The Transformer architecture and its self-attention mechanism have significantly advanced Natural Language Processing and Computer Vision. Self-attention’s ability to capture long-range dependencies makes it invaluable for 3D pose estimation, which requires careful consideration of spatial, temporal, and multi-view information. Recent works effectively leverage Transformers for 3D pose estimation in both single-camera setups [27], [28] and for handling spatiotemporal information within single images [29]–[31]. Additionally, transformers show promise in aggregating multi-view clues via epipolar geometry [3], [32]. Despite the impressive performance of transformers in a variety of tasks, their memory requirements cause an obstacle in processing all spatial, temporal, and multi-view information together. As a result, a group of researchers has adopted a criss-cross attention mechanism to limit each attention layer’s receptive field without sacrificing the network’s overall receptive field [33]. Recent work has also adopted the criss-cross attentions [8] to process temporal and joint information for human 3D pose estimation, showing superior performance compared to parallel or concurrent models.

## III. METHOD

Our method, Upose3D, determines the 3D coordinates of body joints from one or more consecutive image frames captured from multiple viewpoints. Figure 1 depicts an overview of our proposed method. At first, an RLE-based 2D pose estimator (Sec. III-A) extracts 2D keypoints and their corresponding uncertainties from the input images. The keypoints are then projected onto other views using epipolar geometry (Sec. III-B). From there, the pose compiler (Sec. III-C) refines the keypoint locations and

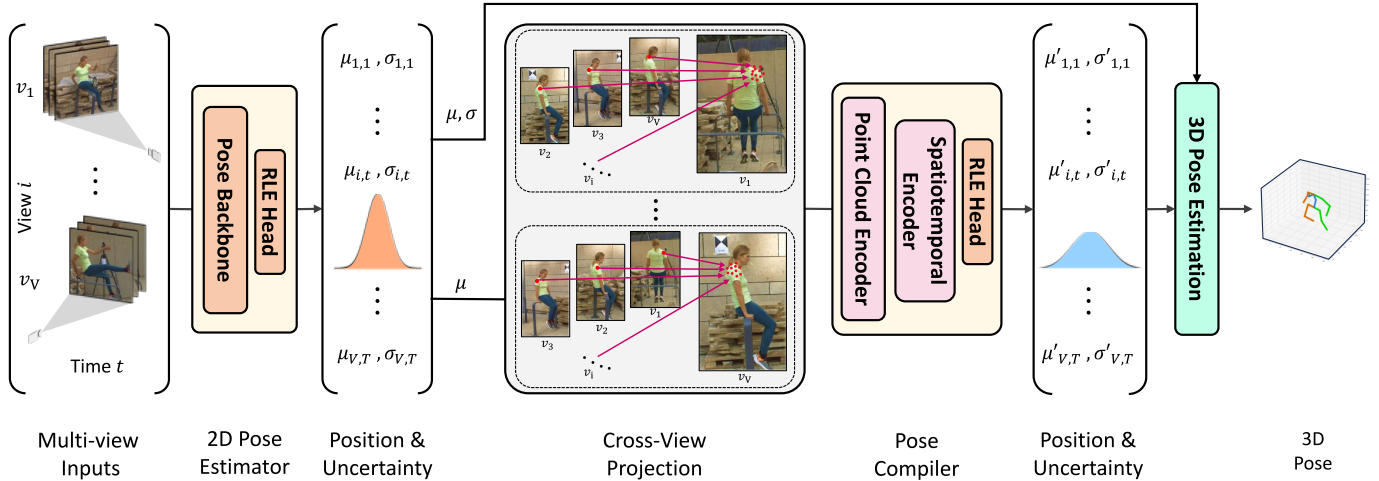


Fig. 1. We illustrate the key stages of UPose3D. It begins with extracting 2D keypoints and uncertainties from the multi-view videos. The keypoints are then projected onto each reference view using epipolar geometry. Our pose compiler is then used to refine the predictions by leveraging cross-view and spatiotemporal information. Finally, the 3D pose is obtained using the keypoint and uncertainty predictions of each stage.

their uncertainties by leveraging spatiotemporal and cross-view information. Lastly, using outputs from the 2D pose estimator and the pose compiler, an iterative refinement stage obtains the final 3D poses (Sec. III-D). We end this section by describing our multi-view training data synthesis (Sec. III-E).

#### A. 2D Pose Estimation

The first step of our method is estimating 2D joint position in each image  $\mathcal{I}_{i,t}$  from all camera views  $i \in \mathcal{V} = \{1, 2, \dots, V\}$  and frames  $t \in \mathcal{T} = \{1, 2, \dots, T\}$ . Similar to [34], [35], our method implements a single layer Residual Log-likelihood Estimation (RLE) head [23] on top of an off-the-shelf backbone (*e.g.*, CPN [36]). Aside from being computationally effective and robust to occlusion, RLE provides uncertainty  $\hat{\sigma}$  for each joint position prediction  $\hat{\mu}$ . Specifically, the RLE predicts a distribution  $P_{\Theta}(x|\mathcal{I})$  that models the probability of the ground-truth keypoints appearing in position  $x$  using a normalizing flow model [37] with learnable parameters  $\Theta$ . The  $\hat{\mu}$  produced by this first module is refined in the next stages by leveraging cross-view and temporal information. The estimated  $\hat{\mu}$ ,  $\hat{\sigma}$ , along with the normalizing flow parameters  $\Theta$ , are also used during our final 3D keypoint estimation process in Sec. III-D.

#### B. Cross-view Projection

Next, we leverage the information from multiple camera views by projecting the 2D keypoints from one view to another using epipolar geometry. We derive a fundamental matrix  $F_{ij} \in \mathbb{R}^{3 \times 3}$  relating two camera views  $i, j \in \mathcal{V}$  from known intrinsic and extrinsic camera parameters. For each predicted keypoint  $\hat{\mu}_j$  in view  $j$ , we obtain the epipolar line in the reference view  $i$  by  $I_{ij} = F_{ij}^T \hat{\mu}_j$  [38]. Next, we find the closest point on  $I_{ij}$  to the keypoint

$\hat{\mu}_i$  in view  $i$ . This point represents the projection of the keypoint from view  $j$  onto the reference view  $i$ . By repeating this cross-view projection for all available views  $i$ , joints  $k \in \mathcal{J} = \{1, 2, \dots, J\}$ , and time frames  $t$ , we create 2D point clouds  $\mathcal{C}_{i,k,t}$  containing the projected keypoint. Finally, for consistency between various scales and views, we normalize the elements of  $\mathcal{C}$  using the subject’s bounding box within their reference view.

#### C. Pose Compiler

The pose compiler module aggregates multi-view information embedded in the 2D point clouds and leverages temporal information (*i.e.*, joint positions across time). As shown in Fig. 1, the pose compiler consists of 2 main parts: a point cloud encoder and a spatiotemporal encoder. The point cloud encoder first extracts a feature vector  $f_{i,k,t}$  that describes a point cloud  $\mathcal{C}_{i,k,t}$ . Our implementation is inspired by the naïve Point Cloud Transformers [39], [40], but we modify its architecture to preserve coordinate information. Specifically, we use multi-head attention and a residual connection from the features of the reference view to the output of the last max-pooling layer. For the detailed architecture of our point cloud encoder, please refer to Fig. 2.

Next, we concatenate the feature vectors from every frame and joint in each reference view  $\{\mathbf{f}_i\}$  with temporal and spatial (*i.e.*, frame and skeleton joint ID) position embeddings. The results are then passed to our spatiotemporal encoder that implements an RLE head to provide position  $\hat{\mu}'_{i,k,t}$  and uncertainty  $\hat{\sigma}'_{i,k,t}$  estimations. Our spatiotemporal encoder is a transformer [41], with specific attention block modifications that accommodate the large dimensionality of the tensors containing all temporal and skeleton information. As detailed in Fig. 2, we replace the standard attention module with criss-cross attentions [8], [33], which approximates full temporal and spatial

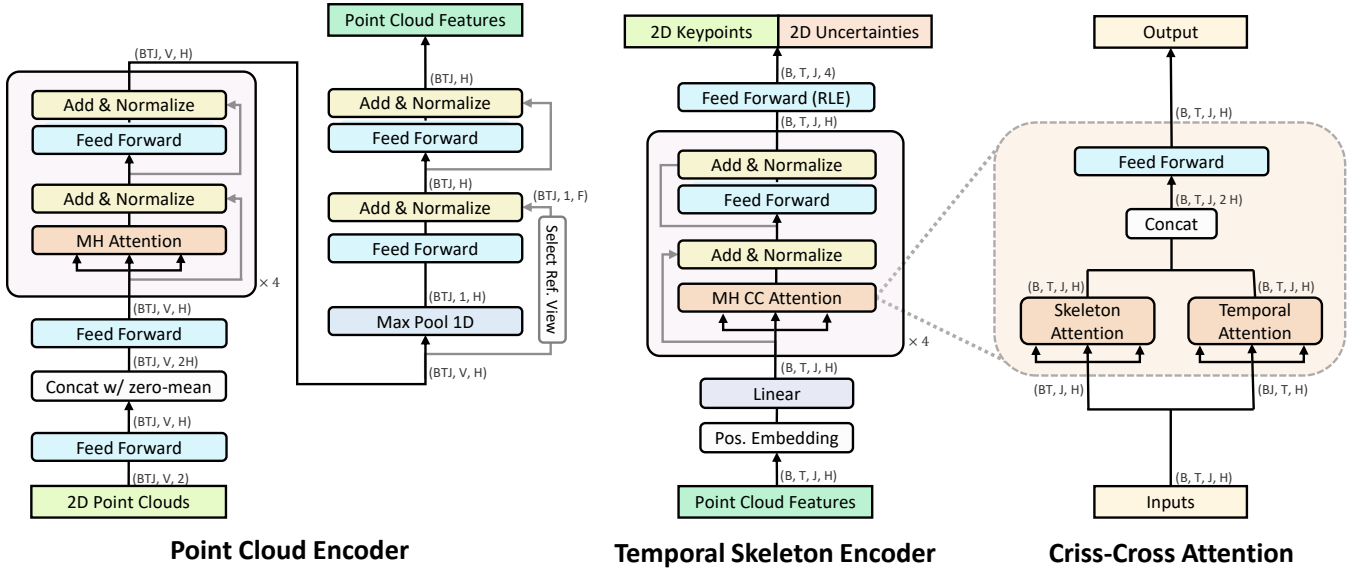


Fig. 2. Architecture of the proposed pose compiler module consisting of a point cloud encoder and a spatiotemporal encoder with criss-cross attention. Tensor sizes depend on the batch size  $B$ , temporal window length  $T$ , number of joints  $J$ , camera views  $V$  and the point cloud feature dimensionality  $H$ .

dependencies while being more memory efficient than full attention.

Accordingly, the cross-view input features  $\{f_i\}$  are first projected into queries, keys, and values ( $Q, K, V \in \mathbb{R}^{T \times J \times 2H}$ ) via a linear layer. Next, we divide them into temporal  $Q_T, K_T, V_T \in \mathbb{R}^{T \times J \times H}$  and spatial groups  $Q_S, K_S, V_S \in \mathbb{R}^{T \times J \times H}$ . The temporal and spatial (skeleton joints) attentions are then calculated in two separate self-attention modules and concatenated before the next feed-forward layer and normalization. As a result of this operation, the receptive field of each transformer layer is the information residing on the spatial and temporal axis, and stacking multiple layers can approximate the full spatiotemporal attention without large computational overhead.

We train the RLE head of the spatiotemporal encoder using the same strategy as [23]. Finally, similarly to Sec. III-A, the RLE head simultaneously maximizes and learns a distribution  $P_{\Theta'}(x|\mathcal{C})$  that represents the probability of the appearance of a keypoint in position  $x$  using a normalizing flow model with learnable parameters  $\Theta'$ . In the next section, we use the estimated  $\hat{\mu}'$ ,  $\hat{\sigma}'$ , and  $\Theta'$  for 3D pose estimation.

### D. 3D Pose Estimation

As the final step, our method obtains the 3D keypoints using position estimates from 2D frames ( $\hat{\mu}, \hat{\sigma}$ ), as well as refined versions from the pose compiler ( $\hat{\mu}', \hat{\sigma}'$ ). Specifically, we use the estimated keypoints as labels when sampling from the associated keypoint density functions ( $P_{\Theta}(x|\mathcal{I})$  and  $P_{\Theta'}(x|\mathcal{C})$ ) during Maximum Likelihood Estimation (MLE). Therefore, the total loss function of MLE

for each joint and each time frame is defined as:

$$\mathcal{L}_{mle} = -\log \prod_{i \in \mathcal{V}} P_{\Theta}(u_i|\mathcal{I}) \Big|_{u_i=\hat{\mu}_i} - \log \prod_{i \in \mathcal{V}} P_{\Theta'}(u_i|\mathcal{C}) \Big|_{u_i=\hat{\mu}'_i}, \quad (1)$$

where  $u_i$  is the projection of variable 3D point  $U$  onto each camera view  $i$ . Minimizing this loss function increases the likelihood of  $U$  appearing close to the ground-truth 3D keypoints  $U_g$  without 3D supervision. To solve this non-convex optimization problem, we initialize  $U$  with a Direct Linear Transformation (DLT) algorithm [38] and iteratively refine it using an optimizer, *i.e.*, L-BFGS [42].

### E. Multi-view Training and Data Synthesis

Our proposed pose compiler does not require 3D annotated data, given that it operates on point clouds. Therefore, we can use animation data to create a synthetic training set. In our In-Distribution (InD) experiments, we use the SMPL+H [43] body model and a Human3.6m [11] specific 17-joint regressor provided by [44]. For our OoD experiments, we use the SMPL-X [45] body model and train a whole-body 133-joint regressor from scratch synthetically on 1000 rendered multi-view images [46].

Let  $r \in \mathbb{R}^{T \times 3}$ ,  $\Theta \in \mathbb{R}^{T \times 55 \times 3 \times 3}$ , and  $\beta \in \mathbb{R}^{16}$  be root position, body joint rotation matrices, and shape parameters from human motion capture data. We begin our multi-view data generation by augmenting the shape parameters with Gaussian noise with a standard deviation equal to the standard deviation of all shape parameters within the datasets. Next, we apply mediolateral mirroring with a 50% chance and randomly rotate the motion sequence around its center. We pass the augmented  $\{r, \Theta, \beta\}$  parameters to the forward-kinematic layer of the SMPL body model to obtain 3D vertices. Lastly, we use the dataset-specific joint regressor on the vertices to extract the 3D keypoints used in the next steps of our pipeline.

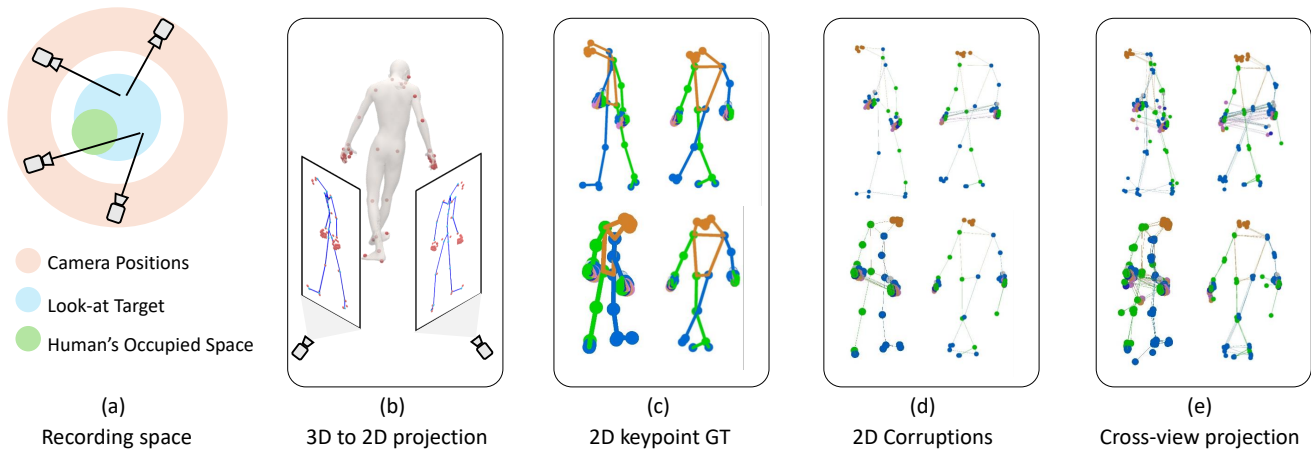


Fig. 3. We illustrate our multi-view data synthesis framework, starting with (a) camera placement in a space surrounding a motion-captured human body; (b) extraction and projection of keypoints onto the synthetic cameras; (c) 2D ground-truth keypoints; (d) data corruption; and (e) cross-view projection to prepare the point cloud training data for our pose compiler.

Next, we simulate a multi-camera recording setup by randomly positioning several cameras in cylindrical space. As depicted in Fig. 3-a, we randomly choose a recording volume size that encircles the space occupied by the human body. To ensure that the subject appears in most cameras, we select the tilt, pitch, and yaw so that they look at a random point in the center of the recording volume while maintaining the correct up direction. Additionally, we limit the camera height to mimic typical multi-view video recording setups.

After obtaining the camera intrinsic and extrinsic parameters, we project the 3D body keypoints onto each camera view (see Fig. 3-b). We use these 2D keypoints as ground-truths  $\mu_g$  to train our pose compiler (see Fig. 3-c). We then add 2D point corruptions to the 2D keypoints, including Gaussian noise with varying standard deviations, simulated occlusions with varying sizes and probabilities, mediolateral flipping, and occasional truncation effects (see Fig. 3-d). Next, we obtain the cross-view projected keypoints (see Fig. 3-e) via the algorithm described in Sec. III-B. Finally, we train our pose compiler using the ground-truth keypoints and point clouds containing noisy 2D data, as depicted in Fig. 4.

## IV. EXPERIMENTS

### A. Datasets

We compare our proposed approach with prior works on the Human3.6m [11] dataset and measure how our method generalizes to different skeleton configurations and unseen outdoor environments using the COCO WholeBody [14] and RICH [12] datasets. The pose compiler is trained using motion capture data from the AMASS dataset [13] to simulate multi-view training data. Finally, we analyze the viewpoint scalability of our approach on the CMU Panoptic [47] dataset. The details of these datasets are as follows:

**Human3.6m.** The Human3.6m [11] dataset is a standard benchmark for evaluating the performance of 3D human

pose estimation solutions in multi-view [6] and single-view [9] settings. We report our InD performance using Protocol-I by training our 2D pose estimator on subjects 1, 5, 6, 7, and 8 and evaluating UPose3D on subjects 9 and 11. We use the same 3D ground-truth keypoints and camera parameters as [5].

**RICH.** Real scenes, Interaction, Contact, and Humans (RICH) dataset [12] is a recently published dataset of multi-view videos with accurate markerless motion captured bodies and scenes. The dataset contains human bodies and 3D-scanned scenes obtained using markerless motion capture technology. The 3D annotations are provided in SMPL-x [45] format, from which we extract 3D ground-truth keypoints for evaluation. We report our OoD performance on the test set, which contains 7 subjects in 52 scenarios and 3 environments, including a construction site, a gym, and a lecture hall.

**COCO WholeBody.** The COCO WholeBody dataset is a large-scale whole-body pose estimation dataset with over 250K samples [14]. This dataset is an extension of Common Objects in COntext (COCO) [15] dataset with the same training and testing splits. The dataset provides 133 2D keypoints (17 for body, 6 for feet, 68 for face, and 42 for hands) on in-the-wild images. We use this dataset to train our 2D pose estimator during OoD experiments.

**CMU Panoptic.** The CMU Panoptic [47] dataset is a large collection of human body poses and interactions recorded from multiple views. The dataset provides videos from 480 VGA and 30 HD cameras and ground-truth 3D poses obtained from markerless 2D pose estimation and triangulation. We use a small subset of the validation set in line with [2] to analyze the scalability of our approach with the addition of camera views.

**AMASS.** The Archive of Motion Capture as Surface Shapes (AMASS) [13] is a large collection of 3D human motion capture datasets. It contains over 40 hours of recording from 300 subjects spanning 11,000 actions. An important contribution of this dataset is the unification of

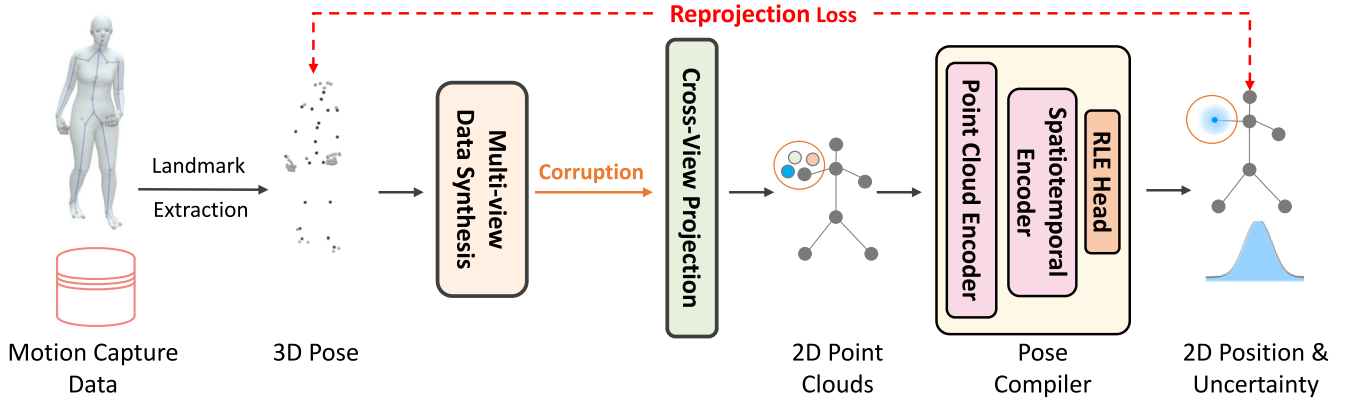


Fig. 4. We illustrate the training routine of our pose compiler using synthetic data generated from human motions.

3D human bodies under the SMPL [43] and SMPL-x [45] parametric models used to train strong motion and pose priors such as VPoser [45] and HuMoR [48]. We only use the training set of this dataset following prior works [45], [48].

### B. Evaluation Metrics

We adopt the standard evaluation metrics used in prior works for our InD experiments on the Human3.6m [11] dataset. Mean Per Joint Position Error (MPJPE) represents the distance between the ground truth and predicted pose in millimeters, while its Procrustes Aligned version (PA-MPJPE) and the Normalized variant (N-MPJPE) show how well the predicted pose fits the ground-truth keypoints after a similarity transformation. Next, we report the translation aligned error (TA-MPJPE) and PA-MPJPE for our OoD experiments on the RICH [12] dataset following prior works [27], [49]–[53].

### C. Implementation Details

We implement our pipeline using PyTorch [54] and MMPose [55]. To compare our method with prior works, we choose a CPN [36] backbone based on ResNet152 [56] with an input size  $384 \times 384$  and an RLE head [23] for 2D pose estimation. We fine-tune our 2D pose estimator jointly on Human3.6m [11] and MPII [57] datasets starting from the weights of the checkpoints provided in [2]. For our OoD experiments, we use an HRNet-W48 [24] with  $384 \times 384$  input size and train it from scratch.

In our point cloud encoder, we use 4 multi-head self-attention blocks, each with 4 attention heads. Additionally, we reduce its hidden dimension to 64 to accommodate the relatively smaller size of our point clouds. Following the point cloud encoder, the features are concatenated with two positional embeddings of size 64 to represent the time frames and different skeleton joints. Our spatiotemporal encoder employs four criss-cross transformer blocks [8], [33] with 4 attention heads each. We set the hidden layer dimension of our transformers to 64 and the hidden dimension of prediction heads to 1024. We then train our

pose compiler module using AdamW optimizer [58] with a batch size of 64 on the AMASS [13] dataset for both OoD and InD evaluations. We use a learning rate of  $4e-5$  with a warm-up factor of  $1e-4$  for the first 500 iterations and a cosine annealing scheduler over the next 20,000 iterations. The network training takes about 6 hours on an NVIDIA 2080 RTX GPU.

Unlike prior works that rely on rendering techniques for synthetic data generation [4], [59], we generate samples online with varying numbers of camera views (up to 8) during training without significant computation overhead. Furthermore, we increase the diversity of the motion capture data by applying several augmentations to the motion capture data before 3D keypoint extraction, such as random 180-degree rotations and mirroring around the mid-hip point.

### D. Baselines

On Human3.6m [11], we compare our UPose3D with methods that infer 3D human keypoints using only 2D supervised models [1], [3], [7], [17], [36], [63]. Additionally, we provide a summary of methods that rely on 3D annotations [2]–[4], [6], [7], [32], [60]–[62] that use ground-truth camera parameters during inference, except for a few [10], [61], [62] that use uncalibrated cameras. We also report a more in-depth comparison with weakly-supervised and semi-supervised approaches [17], [59], [65]–[67], camera-based multi-view methods that do not rely on camera parameters [10], [61], [62], and monocular 3D pose estimation methods [27], [49]–[53]. We also report and compare the performance of our method against triangulation approaches, such as DLT, RANSAC, and RPSM [7]. On the RICH dataset [12], we compare our model with triangulation approaches and replicate the performance of AdaFuse [4], one of the top-performing methods of Human3.6m dataset [11].

## V. RESULTS

### A. In-Distribution Performance

In Table I, we present a comparison of our InD results with other state-of-the-art methods on the Human3.6m

TABLE I

THE COMPARISON OF OUR METHOD IN IN-D SETTINGS AGAINST PRIOR MULTI-VIEW WORKS ON THE FULL TEST SET OF THE HUMAN3.6M DATASET. (-) DENOTES THAT THE ERROR WAS NOT REPORTED IN THE ORIGINAL WORK. THE ERRORS ARE REPORTED IN MM.

Method	Backbone	Frames	MPJPE↓	PA-MPJPE↓	N-MPJPE↓
<i>3D Supervision</i>					
Cross-view Fusion [7]	ResNet152	1	26.2	-	-
Learnable Triangulation [2]	ResNet152	1	20.7	17.0	-
Epipolar Transformers [3]	ResNet152	1	19.0	-	-
Canonical Fusion [60]	ResNet152	1	21.0	-	-
AdaFuse [4]	ResNet152	1	19.5	-	-
TesseTrack [10]	HRNet [24]	5	18.7	-	-
TransFusion [32]	ResNet50	1	25.8	-	-
MTF-Transformer+ [6]	CPN	1	26.5	-	-
MTF-Transformer+ [6]	CPN	27	25.8	-	-
Flex [61]	ResNet152	All	30.2	-	-
Jiang <i>et al.</i> [62]	ResNet152	1	27.8	-	-
<i>2D Supervision</i>					
EpipolarPose [17]	ResNet50	1	55.08	47.91	54.90
AniPose [1], [63]	GT	1	-	75.0	103.0
MetaPose [1]	PoseNet [64]	1	-	32.0	49.0
RPSM [3], [7]	ResNet152	1	31.2	-	-
DLT [7]	ResNet152	1	36.3	-	-
DLT [36]	CPN	1	30.5	27.6	29.8
UPose3D (Ours)	ResNet152	1	31.0	29.0	31.2
UPose3D (Ours)	ResNet152	27	29.9	27.2	29.8
UPose3D (Ours)	CPN	1	26.9	24.1	26.2
UPose3D (Ours)	CPN	27	26.4	23.4	25.6

TABLE II

COMPARISON OF OUR METHOD IN OoD SETTING ON THE RICH [12] DATASET AGAINST PRIOR WORKS. \* DENOTES OUR IMPLEMENTATION OF PRIOR WORKS.

Method	MPJPE↓	PA-MPJPE↓
AdaFuse* [4]	524.0	85.8
HRNet-W48+RANSAC*	338.9	138.9
HRNet-W48+DLT*	66.0	55.1
Ours ( $T = 1$ )	36.2	33.4
Ours ( $T = 27$ )	34.7	32.0

dataset, divided into two categories: methods that are trained directly with 3D annotated data and methods like ours that leverage only 2D supervision. We observe that our method outperforms other methods that rely on 2D supervision. In addition, UPose3D yields results that are competitive with state-of-the-art methods relying on 3D supervision. For example, we achieve similar results to MTF-Transformers, which, like our pose compiler, takes in multi-view and temporal 2D keypoints as input, but estimates the 3D poses directly using a deep network with 10.1M parameters. This indicates that our proposed pose compiler module and training strategies are effective in obtaining precise keypoint position estimations.

We also experiment with different 2D pose estimator backbones. We see that the choice of backbone is an important factor for accuracy and that CPN is preferred over ResNet152. Interestingly, a vanilla triangulation algorithm (DLT) can outperform prior works given accurate 2D predictions from strong pose estimators. Combining strong pose estimators with our method yields even better

performance. For instance, UPose3D improves the MPJPE by 3.6 mm when compared to vanilla triangulation using a CPN backbone (DLT+CPN). Finally, we observe that increasing the temporal frame window positively impacts performance, reducing MPJPE by 0.5 mm when using 27 frames instead of a single frame.

### B. Out-of-Distribution Generalization

In order to evaluate the performance of UPose3D in OoD settings, we compare it to the best-performing baseline on the Human3.6m [11] dataset, namely AdaFuse [4]. Additionally, we report the results for triangulation techniques applied to 2D pose estimators Table II. In this experiment setup, none of the models nor their components are trained on the RICH [12] dataset. First, we observe that our method obtains the best results, achieving half of the error of the next best method. Additionally, we observe that AdaFuse performs poorly on this dataset despite being considered state-of-the-art on Human3.6m [11] dataset. Our analysis of AdaFuse performance on different clips of RICH [12] dataset indicates that this method performs well only if all the viewpoints' predictions are within a reasonable range, whereas occasional noisy predictions cause large triangulation errors. In conclusion, we believe that by training on limited in-studio datasets, methods such as AdaFuse fail to generalize well to outdoor and in-the-wild environments. In contrast, our approach uses synthetic data and performs consistently when applied to unseen datasets.

TABLE III

ADDITIONAL COMPARISONS WITH PRIOR WORKS ON THE FULL TEST SET OF THE HUMAN3.6M DATASET IN InD SETTINGS. (-) DENOTES THAT THE ERROR WAS NOT REPORTED IN THE ORIGINAL WORK.

Method	Supervision	Multi-view	Frames	MPJPE $\downarrow$	PA-MPJPE $\downarrow$	N-MPJPE $\downarrow$
Rhodin <i>et al.</i> [65]	3D	$\times$	1	66.8	51.6	63.3
Rhodin <i>et al.</i> [65]	Weakly 3D	$\times$	1	-	65.1	80.1
EpipolarPose [17]	Weakly 3D	$\times$	1	55.08	47.91	54.90
CanonPose [66]	Weakly 3D	$\times$	1	-	53.0	82.0
Gong <i>et al.</i> [59]	Synthetic 3D	$\checkmark$	1	53.8	42.4	-
BKinD-3D [67]	3D Discovery	$\checkmark$	20	125.0	105.0	-
UPose3D (Ours)	2D	$\checkmark$	1	26.9	24.1	26.2
UPose3D (Ours)	2D	$\checkmark$	27	26.4	23.4	25.6

TABLE IV

ADDITIONAL COMPARISON OF OUR METHOD IN OoD SETTING ON RICH DATASET AGAINST PRIOR WORKS. \* DENOTES OUR REPLICATION OF PRIOR WORKS.

Method	MPJPE $\downarrow$	PA-MPJPE $\downarrow$	OoD	Multi-view	Output
SA-HMR [53]	93.9	-	$\times$	$\times$	SMPL
IPMAN-R [52]	79.0	47.6	$\times$	$\times$	SMPL
METRO [27]	98.8	-	$\times$	$\times$	SMPL
METRO [27]	129.6	-	$\checkmark$	$\times$	SMPL
SPIN [51]	112.2	71.5	$\checkmark$	$\times$	SMPL
PARE [50]	107.0	73.1	$\checkmark$	$\times$	SMPL
CLIFF [49]	107.0	67.2	$\checkmark$	$\times$	SMPL
SkelFormer [46]	44.2	35.6	$\checkmark$	$\checkmark$	SMPL
Ours ( $T = 1$ )	36.2	33.4	$\checkmark$	$\checkmark$	3D Keypoints
Ours ( $T = 27$ )	34.7	32.0	$\checkmark$	$\checkmark$	3D Keypoints

TABLE V

ABLATION EXPERIMENTS ON THE HUMAN3.6M DATASET WITH  $T = 27$ .

Method	MPJPE $\downarrow$	PA-MPJPE $\downarrow$
<b>UPose3D</b>	26.42	23.42
w/o compiler	37.14	33.90
w/o image branch	69.90	50.97
w/o compiler uncertainty	26.42	23.58
w/o image uncertainty	27.61	24.88
w/o uncertainty	48.11	41.20
w/o image branch	77.25	54.02
w/o compiler	30.48	27.63

### C. Additional Baselines and Comparisons

Table III complements Table I by providing more comparisons with prior works on the Human3.6m [11] dataset. Here, we include 3D keypoint estimation approaches regardless of their input modality or supervision type in InD settings. We observe that our method outperforms all of the other approaches despite only using 2D supervision. Additionally, in Table IV, we compare our work with prior research on the RICH [12] dataset. Since this dataset was recently published, only monocular 3D body modeling techniques have reported their performance on this dataset. Here, we observe that our method outperforms the majority of prior works. More importantly, when comparing Table III and Table IV we notice that our method performs consistently on InD and OoD data, showing generalizability across in-studio and outdoor environments.

### D. Ablation Study

To investigate the impact of each component of UPose3D, we systematically remove them and report the results of our method with a CPN backbone on the test set of Human3.6m [11]. We perform all our experiments using a model trained with a temporal window of 27 frames. Accordingly, we first ablate the effect of our pose compiler and uncertainty modeling. Next, we study the details of our pipeline to evaluate its performance under different inputs, network architectures, and initialization strategies for 3D keypoint estimation. We further investigate the impact of temporal length, our spatiotemporal encoder’s architecture, different formulations of the point clouds, and our initialization strategy for 3D keypoint estimation.

**Effect of Pose Compiler.** Our UPose3D employs the pose compiler module to improve the keypoint and uncertainty predictions using cross-view and spatiotemporal information. By ablating this component, we use the original keypoints and uncertainties predicted by our 2D pose estimator to perform MLE. As shown in Table V, this experiment results in an additional 9.28 *mm* error resulting in a higher error compared to the DLT algorithm (See Table I). This shows the effectiveness of our pose compiler for 3D pose estimation using normalizing flows.

**Effect of Image Branch.** We study the impact of the image branch by removing it from the pipeline, which causes a significant rise in the error as seen in Table I. This indicates the significance of keeping the original predictions for the final estimation.

**Effect of Uncertainty Modeling.** We employ the nor-



TABLE VI

ADDITIONAL ABLATION STUDY ON HUMAN3.6M DATASET. WE ONLY REPORT THE COMPUTATION COST OF OUR POSE COMPILER AND EXCLUDE THE CPN [36] NETWORK (WITH 5.16T FLOPs AND 64.87M PARAMETERS) FOR 27 FRAMES OF 4 VIEWS.

Method	MPJPE $\downarrow$	PA-MPJPE $\downarrow$	Param.(M) $\downarrow$	Time(s) $\downarrow$	FLOPs(G) $\downarrow$
<b>UPose3D</b> ( $T = 27, \text{Tol.} = 10^{-3} \text{ mm}$ )	26.42	23.42	65.407	10.1	2.04
w/ zero init	28.51	32.85	65.407	12.5	2.04
w/ zero init ( $\text{Tol.} = 10^{-6} \text{ mm}$ )	26.42	23.42	65.407	28.9	2.04
w/ $T = 243$	33.17	25.11	65.430	10.9	20.18
w/ concurrent attention	26.57	23.61	65.391	10.3	2.01
w/ full attention	26.50	23.57	65.322	10.3	2.28
w/ full attention ( $T = 243$ )	34.97	28.60	65.336	10.3	51.56
w/ epipolar line	26.46	23.45	65.407	10.1	2.04
w/ relative camera pos. emb.	26.37	23.43	65.407	10.2	2.04

malizing flows of our RLE heads during the MLE loss minimization stage to incorporate the uncertainties of our predictions toward improving the model’s robustness. To study the effect of uncertainty modeling, we remove them from the 2D pose estimator and pose compiler branches. Accordingly, we first remove the uncertainties from our pose compiler and replace our likelihood loss function (Eq. (1)) with a reprojection distance loss. Table I shows that the PA-MPJPE error slightly rises, but the MPJPE remains unchanged. Similarly in the next experiment, we remove the image pose estimator uncertainties. This ablation experiment results in 1.2 *mm* rise in the error. Finally, we completely remove the uncertainties from both branches, effectively reducing our problem to a classic triangulation problem without confidence that can be solved via DLT algorithm. As a result, we find the 3D keypoints using a DLT algorithm given the keypoints from each branch. This variation shows over 20 *mm* higher error than UPose3D. In our final two experiments, we analyze the accuracy of each keypoint branch without uncertainty using a DLT triangulation algorithm. The first experiment obtains the highest error in the absence of uncertainties and image pose estimator, while the second experiment results in the same performance of a simple DLT algorithm without cross-view fusion.

**Random Initialization.** We use L-BFGS [42] optimization algorithm to iteratively solve the 3D keypoint MLE. To speed up this process, we stop the optimization when the changes of our optimization variables, namely  $U$ , are less than a specific tolerance ( $\text{Tol.} = 0.001 \text{ mm}$ ). We speed up the optimization process even further by using a DLT algorithm to initialize the 3D points  $U$ . Table VI first examines the effect of our initialization strategy when  $U$  is initialized to zero, and the tolerance remains unchanged, showing a significant rise in the 3D keypoint estimation error and inference time. Next, Table VI shows that by lowering the tolerance, zero-initialization performs similarly to our proposed strategy, but at 3 times more inference time. Therefore, we conclude that unlike prior works [1], our method is not reliant on initialization and the initialization only speeds up the estimation process. This may be due to the smooth nature of the uncertainty distributions learned by the normalizing flows [23].

**Longer Temporal Window.** We study the computational cost and performance impact of very long temporal context size. Following [9], we report the performance of UPose3D when 243 frames, as opposed to 27 frames, are used to infer the 3D keypoints of the center frame in Table VI. This new model takes 10 times more FLOPs to compute and does not perform as well as our original model. This may be because our synthetic data augmentations and corruption strategies are tuned for smaller time windows as longer context sizes were not in our considerations. Our observations of the training and validation losses also show signs of overfitting during training for longer time windows. As extremely long context sizes are not in the scope of this paper, we do not tune these models and leave them for future research.

**Pose Compiler Architecture.** We compare the effect of our criss-cross attention modules with vanilla (full) and concurrent attention. Table VI shows that criss-cross attention outperforms the other two designs while requiring less computation (FLOPs) than full attention. Additionally, we observe that on the extreme case of very long temporal context sizes ( $T = 243$ ), criss-cross attention still outperforms full attention models by 1.8 *mm* while requiring 60% less computations.

**Inputs of Pose Compiler.** Finally, we investigate the effect of different point cloud formation strategies in our pipeline. Specifically, we aim to study the impact of appending a relative camera position embedding, inspired by [6], to the cross-projected 2D keypoints while creating the point clouds. Accordingly, in our first experiment, we concatenate the epipolar line parameters of other views to the point cloud of the reference view. Similarly, in our second experiment, we concatenate the relative position of the other cameras to the input point cloud as well. However, as shown in Table VI, adding extra inputs does not have a large impact on the performance.

### E. Computation

Table VI shows the inference time, computational cost, and the number of parameters of our network. We observe that our pose compiler is significantly smaller than a single 2D pose estimator, taking less than 1% of the total parameter count. Additionally, in Table VII, we present

TABLE VII  
MODEL PARAMETERS.

Method	Parameters M)
Learnable Triangulation [2]	81
Epipolar Transformers [3]	69
MTF-Transformers [6]	72
AdaFuse [4]	69
Ours	65

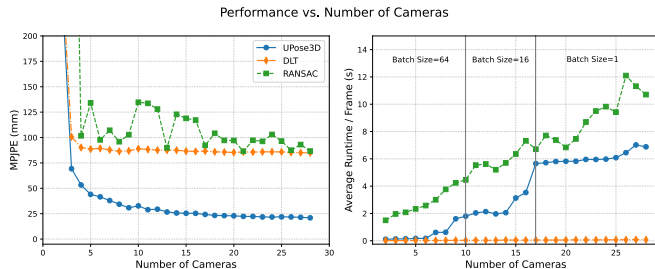


Fig. 5. We demonstrate the scalability of UPose3D to the number of cameras and its Runtime.

the number of parameters of our method in comparison to state-of-the-art 3D pose estimation methods. We show that our method is considerably lighter than prior works.

#### F. Viewpoint Scalability

To test the scalability of our method with viewpoints, we evaluate it with different numbers of cameras on the CMU Panoptic [47] dataset and present the results in Fig. 5. For this experiment, we use the HRNet-W48 [24] backbone similar to our OoD experiments to analyze scalability in in-the-wild scenarios. Additionally, we report the error and runtime of two triangulation techniques, RANSAC and DLT, for comparison. We tune the RANSAC implementation of [2] and run it for 20 iterations. The left figure shows that as the number of views increases, the error of UPose3D continuously improves while DLT and RANSAC reach a plateau at around 85 mm. In the right figure, we show that the inference time of our pipeline with a single batch size remains less than RANSAC. However, increasing the batch size causes both improvements and variability in the runtime at the cost of more computation memory during MLE.

#### G. Qualitative Analysis

Fig. 6 depicts a few challenging examples and shows the outputs of our method. Specifically, by sampling it in every pixel, we demonstrate the output likelihood of keypoints from the 2D pose estimator and our pose compiler as heatmaps. Despite choosing challenging scenes, we observe that the predictions of our method are still close to the ground-truth keypoints, indicating that our method does not produce any significant outliers within its output even on the unseen samples of RICH [12] dataset. Additionally, we observe that the 2D pose estimator generally results

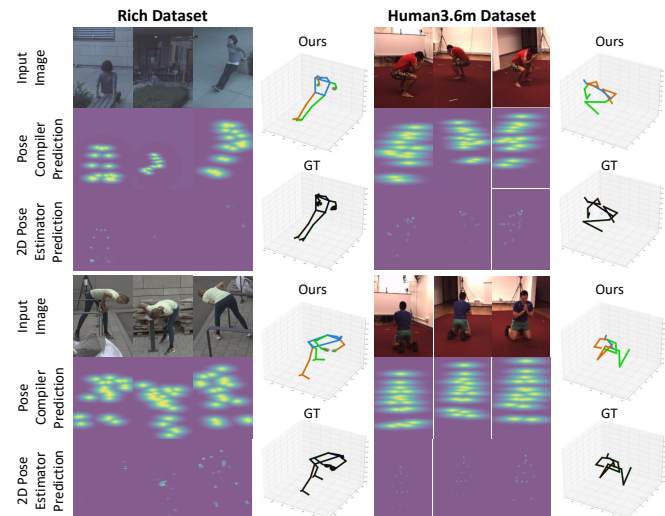


Fig. 6. Illustration of UPose3D on Human3.6m [11] (right) and RICH [12] (left) datasets, showing the accurate 3D pose estimated by our UPose3D (top) compared to ground-truth (bottom). The output keypoint distributions from our 2D pose estimator and pose compiler are also demonstrated as heatmaps.

in more refined predictions and sharper uncertainty distributions, while our pose compiler outputs a coarser distribution. Moreover, our method typically depicts higher horizontal uncertainties, which may be due to the human motions across several frames.

In Fig. 7, Fig. 8, and Fig. 9, we demonstrate more examples of our UPose3D on Human3.6m [11] dataset to showcase its visual fidelity in comparison to ground-truth keypoints and AdaFuse [4] during InD evaluation scheme. Additionally, we provide several visual examples of UPose3D results in Fig. 10, Fig. 11, and Fig. 12 in comparison to our implementation of AdaFuse [4] in OoD settings on the RICH [12] dataset. Unlike Fig. 6, to better visualize the sharp keypoint distribution output of our 2D pose estimators, we show the logarithm of heatmaps in all figures for the 2D pose estimators. We observe that Our method performs consistently in both settings, while AdaFuse fails to correctly predict the human keypoints in some OoD samples.

## VI. CONCLUSION

This paper presents UPose3D, a multi-view 3D human pose estimation method designed to address the challenges in generalization, scalability, and over-reliance on real-world 3D annotated data. It includes a novel cross-view fusion strategy that scales well with varying camera numbers and volume sizes. Additionally, UPose3D integrates a pose compiler that learns to predict keypoint positions and uncertainties given the cross-view and temporal information. This module is trained using our online multi-view data synthesis strategy. Finally, the uncertainties and predicted key points from two sources of image branch and pose compiler are used in an uncertainty-aware 3D human pose estimation algorithm. UPose3D outperforms state-of-the-art approaches in OoD evaluations while achieving

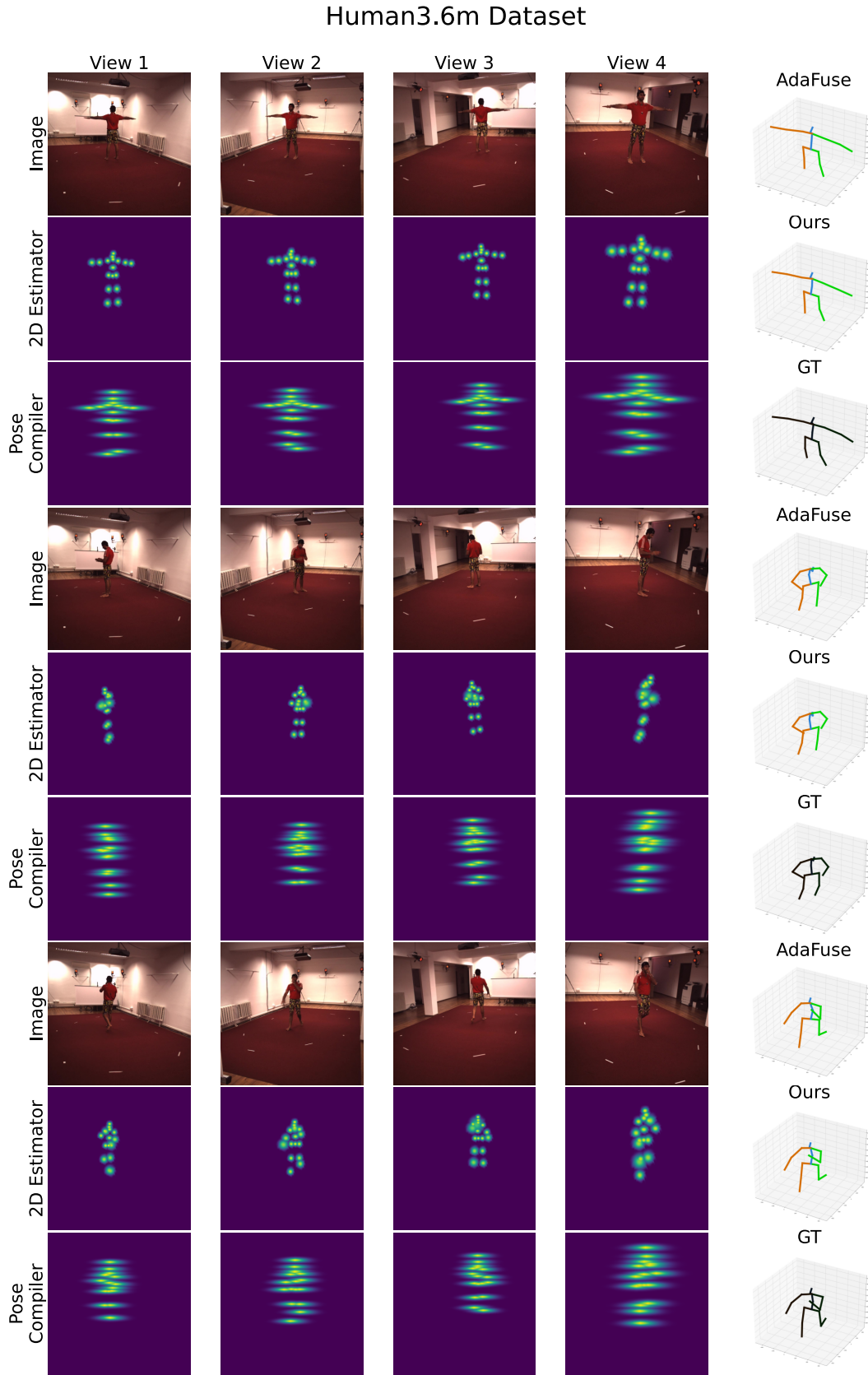


Fig. 7. Example output of our proposed UPose3D pipeline in comparison to AdaFuse [4] is presented in the InD evaluation scheme on the Human3.6m [11] dataset.

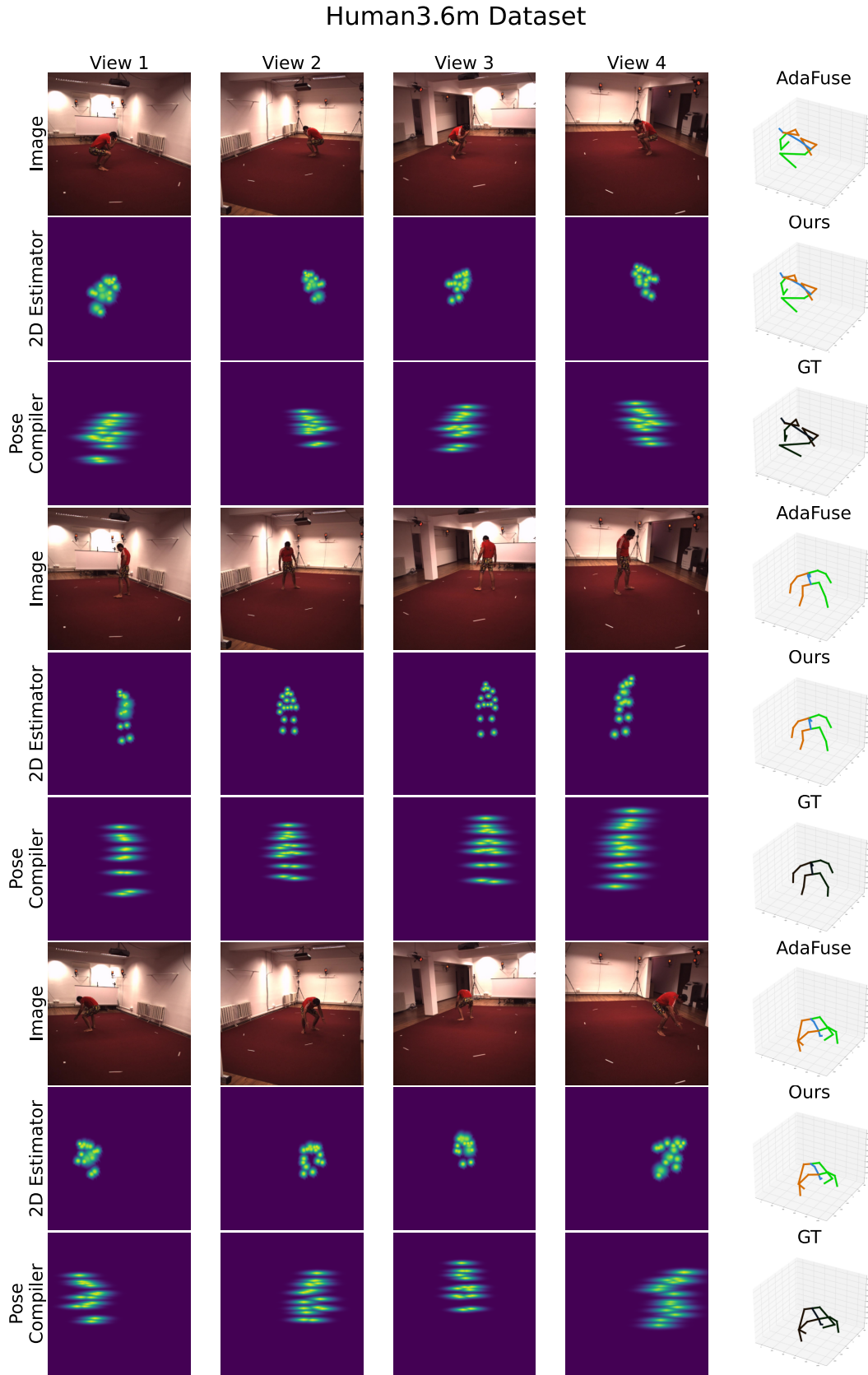


Fig. 8. Example output of our proposed UPose3D pipeline in comparison to AdaFuse [4] is presented in the InD evaluation scheme on the Human3.6m [11] dataset.

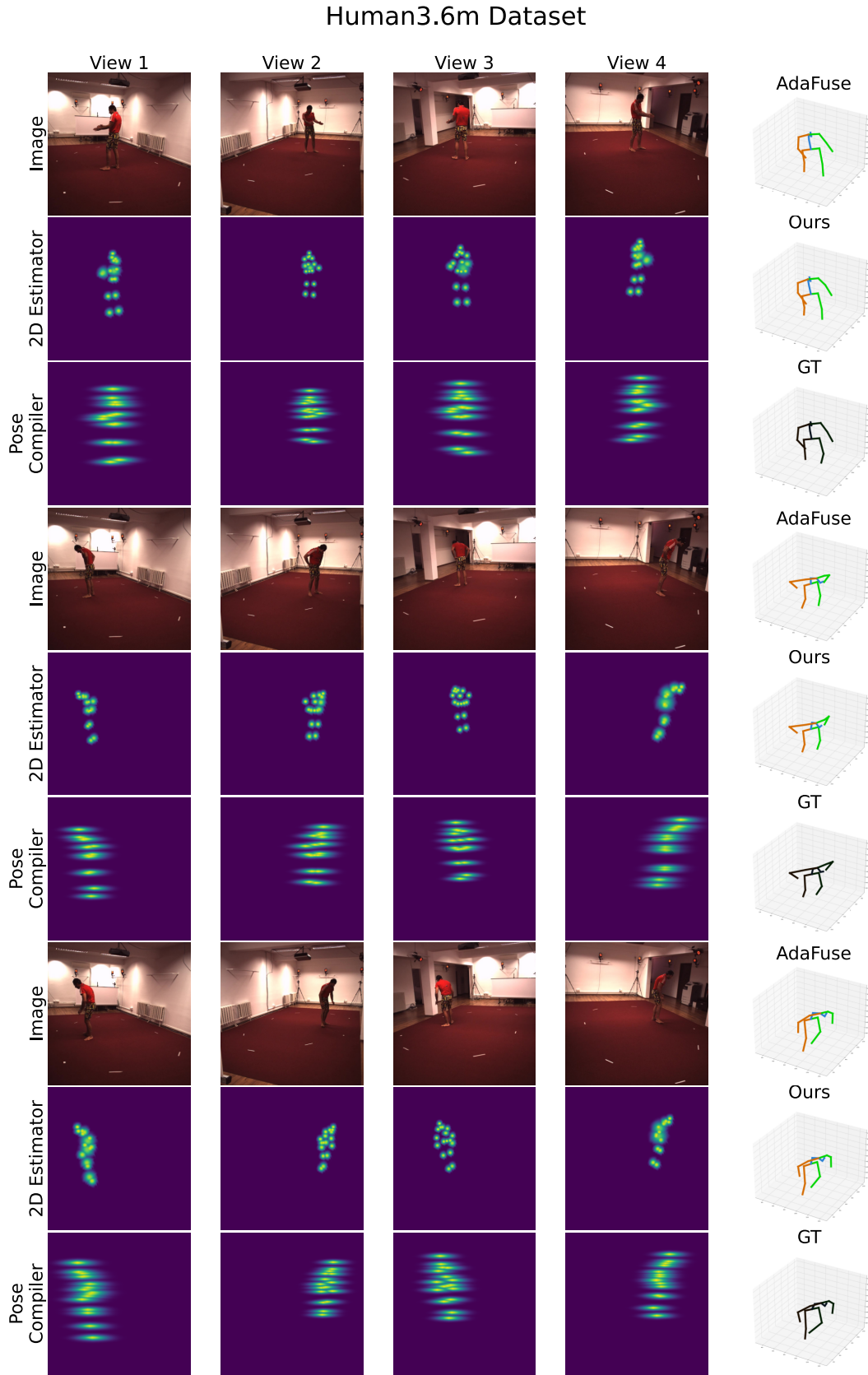


Fig. 9. Example output of our proposed UPose3D pipeline in comparison to AdaFuse [4] is presented in the InD evaluation scheme on the Human3.6m [11] dataset.

## RICH Dataset

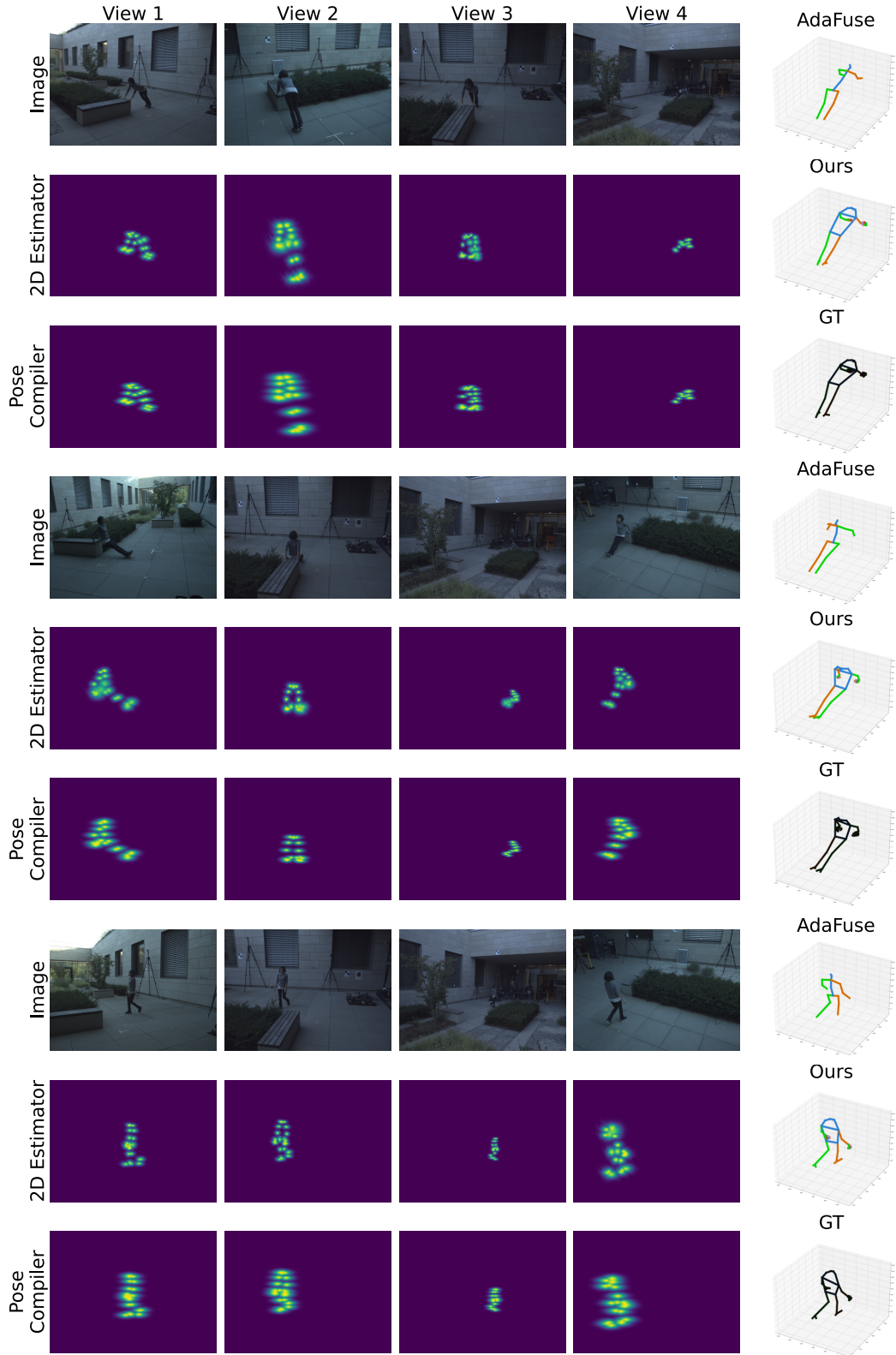


Fig. 10. Example output of our proposed UPose3D pipeline in comparison to AdaFuse [4] is presented in the OoD evaluation scheme on the RICH [12] dataset. The first and second samples show the effectiveness of our approach in solving occlusions for detecting hands and feet.

## RICH Dataset

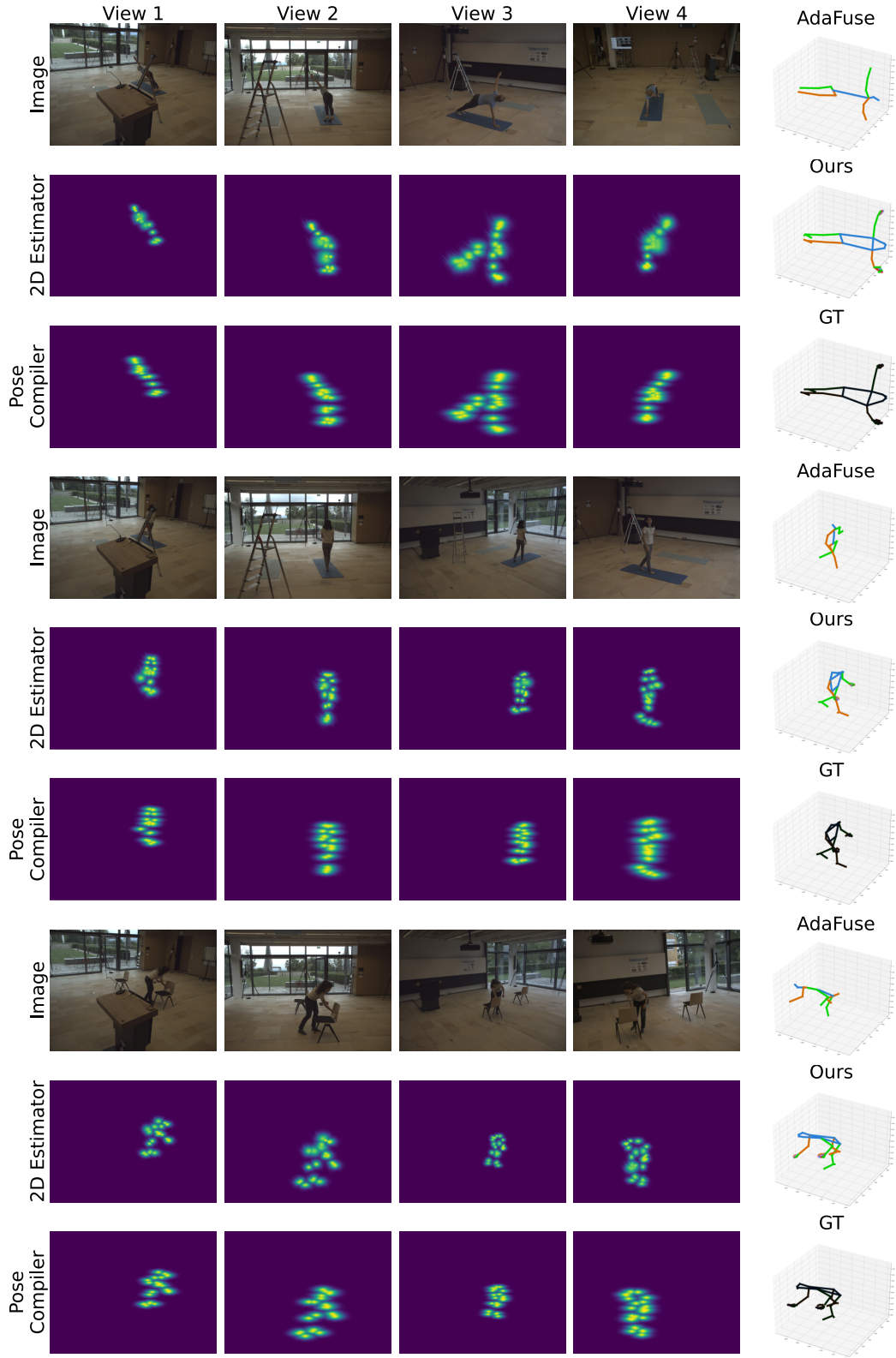


Fig. 11. Example output of our proposed UPose3D pipeline in comparison to AdaFuse [4] is presented in the OoD evaluation scheme on the RICH [12] dataset. The first sample illustrates a challenging input with a rare posture, where both AdaFuse and our method successfully predict the correct posture.

## RICH Dataset

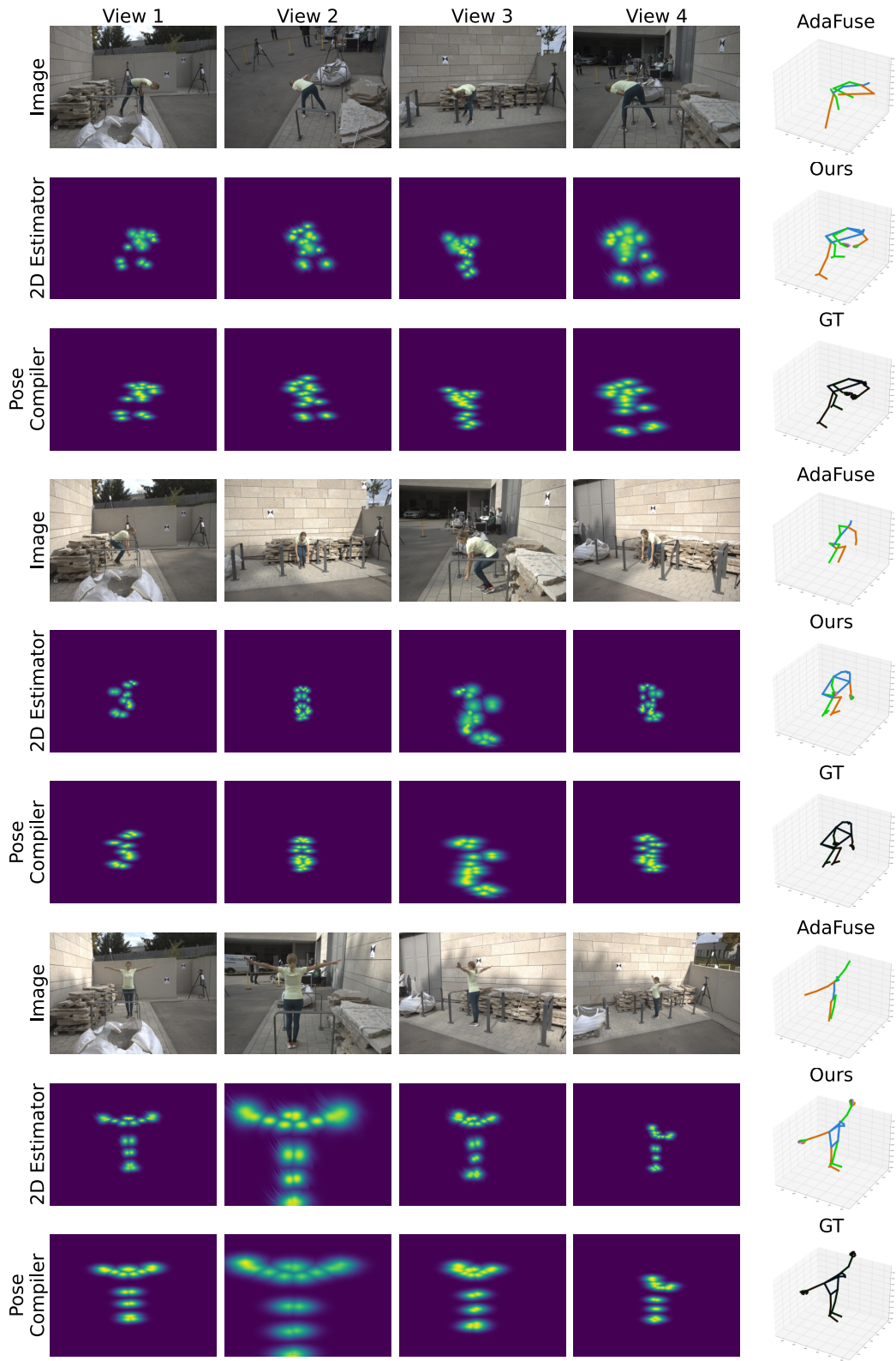


Fig. 12. Example output of our proposed UPose3D pipeline in comparison to AdaFuse [4] is presented in the OoD evaluation scheme on the RICH [12] dataset. We observe that our method outperforms AdaFuse in the first and third samples.



competitive results to in-distribution methods without requiring annotated 3D pose data. In conclusion, UPose3D may positively impact applications in sports analysis and health care, where performance and robustness are crucial. **Limitations and Future Work.** Our primary focus in this paper was the fidelity of estimated output 3D poses from multi-view inputs without requiring 3D supervision. We acknowledge, however, that our method could be optimized for *real-time* applications. A promising avenue to achieve faster inference involves the exploration of specialized second-order optimizers that use a deep-learning neural network to estimate the Hessian matrix during likelihood maximization. Furthermore, given the importance of uncertainty modeling in our performance, it may be possible to reach better robustness by introducing additional sources of constraints. For example, a depth estimation network in each view, as well as a trajectory prediction network, can be used as an additional term in the likelihood function to mitigate the effect of outliers and noisy predictions in 2D pose estimators.

#### ACKNOWLEDGMENT

This work was partially funded by Mitacs through the Accelerate program.

#### REFERENCES

- [1] B. Usman, A. Tagliasacchi, K. Saenko, and A. Sud, “Metapose: Fast 3d pose from multiple views without 3d supervision,” in *IEEE/CVF Conference on Computer Vision and Pattern Recognition (CVPR)*, 2022, pp. 6759–6770.
- [2] K. Isakov, E. Burkov, V. Lempitsky, and Y. Malkov, “Learnable triangulation of human pose,” in *IEEE/CVF International Conference on Computer Vision (ICCV)*, 2019, pp. 7718–7727.
- [3] Y. He, R. Yan, K. Fragkiadaki, and S.-I. Yu, “Epipolar transformers,” in *IEEE/CVF Conference on Computer Vision and Pattern Recognition (CVPR)*, 2020, pp. 7779–7788.
- [4] Z. Zhang, C. Wang, W. Qiu, W. Qin, and W. Zeng, “Adafuse: Adaptive multiview fusion for accurate human pose estimation in the wild,” *International Journal of Computer Vision*, vol. 129, pp. 703–718, 2021.
- [5] J. M. Martínez-Otzeta, I. Rodríguez-Moreno, I. Mendiáldua, and B. Sierra, “Ransac for robotic applications: A survey,” *Sensors*, vol. 23, no. 1, p. 327, 2022.
- [6] H. Shuai, L. Wu, and Q. Liu, “Adaptive multi-view and temporal fusing transformer for 3d human pose estimation,” *IEEE Transactions on Pattern Analysis and Machine Intelligence*, vol. 45, no. 4, pp. 4122–4135, 2022.
- [7] H. Qiu, C. Wang, J. Wang, N. Wang, and W. Zeng, “Cross view fusion for 3d human pose estimation,” in *IEEE/CVF International Conference on Computer Vision (ICCV)*, 2019, pp. 4342–4351.
- [8] Z. Tang, Z. Qiu, Y. Hao, R. Hong, and T. Yao, “3d human pose estimation with spatio-temporal criss-cross attention,” in *IEEE/CVF Conference on Computer Vision and Pattern Recognition (CVPR)*, 2023, pp. 4790–4799.
- [9] W. Zhu, X. Ma, Z. Liu, L. Liu, W. Wu, and Y. Wang, “Motionbert: A unified perspective on learning human motion representations,” in *IEEE/CVF International Conference on Computer Vision (ICCV)*. IEEE, 2023, pp. 15 085–15 099.
- [10] N. D. Reddy, L. Guigues, L. Pishchulin, J. Eledath, and S. G. Narasimhan, “Tesseract: End-to-end learnable multi-person articulated 3d pose tracking,” in *IEEE/CVF Conference on Computer Vision and Pattern Recognition (CVPR)*, 2021, pp. 15 190–15 200.
- [11] C. Ionescu, D. Papava, V. Olaru, and C. Sminchisescu, “Human3.6m: Large scale datasets and predictive methods for 3d human sensing in natural environments,” *IEEE Transactions on Pattern Analysis and Machine Intelligence*, vol. 36, no. 7, pp. 1325–1339, 2013.
- [12] C.-H. P. Huang, H. Yi, M. Höschle, M. Safroshkin, T. Alexiadis, S. Polikovsky, D. Scharstein, and M. J. Black, “Capturing and inferring dense full-body human-scene contact,” in *IEEE/CVF Conference on Computer Vision and Pattern Recognition (CVPR)*, 2022, pp. 13 274–13 285.
- [13] N. Mahmood, N. Ghorbani, N. F. Troje, G. Pons-Moll, and M. J. Black, “Amass: Archive of motion capture as surface shapes,” in *IEEE/CVF International Conference on Computer Vision (ICCV)*, 2019, pp. 5442–5451.
- [14] S. Jin, L. Xu, J. Xu, C. Wang, W. Liu, C. Qian, W. Ouyang, and P. Luo, “Whole-body human pose estimation in the wild,” in *European Conference on Computer Vision (ECCV)*. Springer, 2020, pp. 196–214.
- [15] T.-Y. Lin, M. Maire, S. Belongie, J. Hays, P. Perona, D. Ramanan, P. Dollár, and C. L. Zitnick, “Microsoft coco: Common objects in context,” in *European Conference on Computer Vision (ECCV)*. Springer, 2014, pp. 740–755.
- [16] K. Bartol, D. Bojanić, T. Petković, and T. Pribanić, “Generalizable human pose triangulation,” in *IEEE/CVF Conference on Computer Vision and Pattern Recognition (CVPR)*, 2022, pp. 11 028–11 037.
- [17] M. Kocabas, S. Karagoz, and E. Akbas, “Self-supervised learning of 3d human pose using multi-view geometry,” in *IEEE/CVF Conference on Computer Vision and Pattern Recognition (CVPR)*, 2019, pp. 1077–1086.
- [18] Y. Yao, Y. Jafarian, and H. S. Park, “Monet: Multiview semi-supervised keypoint detection via epipolar divergence,” in *IEEE/CVF International Conference on Computer Vision (ICCV)*, 2019, pp. 753–762.
- [19] M. Kocabas, N. Athanasiou, and M. J. Black, “Vibe: Video inference for human body pose and shape estimation,” in *IEEE/CVF Conference on Computer Vision and Pattern Recognition (CVPR)*, 2020, pp. 5253–5263.
- [20] K. Holmquist and B. Wandt, “Diffpose: Multi-hypothesis human pose estimation using diffusion models,” in *IEEE/CVF International Conference on Computer Vision (ICCV)*, 2023, pp. 15 977–15 987.
- [21] L. Bramlage, M. Karg, and C. Curio, “Plausible uncertainties for human pose regression,” in *IEEE/CVF International Conference on Computer Vision (ICCV)*, 2023, pp. 15 133–15 142.
- [22] J. N. Kundu, S. Seth, P. YM, V. Jampani *et al.*, “Uncertainty-aware adaptation for self-supervised 3d human pose estimation,” in *IEEE/CVF Conference on Computer Vision and Pattern Recognition (CVPR)*, 2022, pp. 20 448–20 459.
- [23] J. Li, S. Bian, A. Zeng, C. Wang, B. Pang, W. Liu, and C. Lu, “Human pose regression with residual log-likelihood estimation,” in *IEEE/CVF International Conference on Computer Vision (ICCV)*, 2021, pp. 11 025–11 034.
- [24] K. Sun, B. Xiao, D. Liu, and J. Wang, “Deep high-resolution representation learning for human pose estimation,” in *IEEE/CVF Conference on Computer Vision and Pattern Recognition (CVPR)*, 2019, pp. 5693–5703.
- [25] Z. Cao, T. Simon, S.-E. Wei, and Y. Sheikh, “Realtime multi-person 2d pose estimation using part affinity fields,” in *IEEE/CVF Conference on Computer Vision and Pattern Recognition (CVPR)*, 2017, pp. 7291–7299.
- [26] Y. Li, S. Yang, P. Liu, S. Zhang, Y. Wang, Z. Wang, W. Yang, and S.-T. Xia, “Simcc: A simple coordinate classification perspective for human pose estimation,” in *European Conference on Computer Vision (ECCV)*. Springer, 2022, pp. 89–106.
- [27] K. Lin, L. Wang, and Z. Liu, “End-to-end human pose and mesh reconstruction with transformers,” in *IEEE/CVF Conference on Computer Vision and Pattern Recognition (CVPR)*, 2021, pp. 1954–1963.
- [28] Y. Zhu, X. Xu, F. Shen, Y. Ji, L. Gao, and H. T. Shen, “Posegtac: Graph transformer encoder-decoder with atrous convolution for 3d human pose estimation,” in *International Joint Conference on Artificial Intelligence (IJCAI)*, 2021, pp. 1359–1365.
- [29] A. Llopart, “Liftformer: 3d human pose estimation using attention models,” *arXiv preprint arXiv:2009.00348*, 2020.
- [30] W. Li, H. Liu, H. Tang, P. Wang, and L. Van Gool, “Mhformer: Multi-hypothesis transformer for 3d human pose estimation,” in *IEEE/CVF Conference on Computer Vision and Pattern Recognition (CVPR)*, 2022, pp. 13 147–13 156.

- [31] C. Zheng, S. Zhu, M. Mendieta, T. Yang, C. Chen, and Z. Ding, "3d human pose estimation with spatial and temporal transformers," in *IEEE/CVF International Conference on Computer Vision (ICCV)*, 2021, pp. 11 656–11 665.
- [32] H. Ma, L. Chen, D. Kong, Z. Wang, X. Liu, H. Tang, X. Yan, Y. Xie, S.-Y. Lin, and X. Xie, "Transfusion: Cross-view fusion with transformer for 3d human pose estimation," *arXiv preprint arXiv:2110.09554*, 2021.
- [33] Z. Huang, X. Wang, L. Huang, C. Huang, Y. Wei, and W. Liu, "Ccnnet: Criss-cross attention for semantic segmentation," in *IEEE/CVF International Conference on Computer Vision (ICCV)*, 2019, pp. 603–612.
- [34] J. Li, S. Bian, C. Xu, Z. Chen, L. Yang, and C. Lu, "Hybrik-x: Hybrid analytical-neural inverse kinematics for whole-body mesh recovery," *arXiv preprint arXiv:2304.05690*, 2023.
- [35] S. K. Dwivedi, C. Schmid, H. Yi, M. J. Black, and D. Tzionas, "Poco: 3d pose and shape estimation with confidence," *arXiv preprint arXiv:2308.12965*, 2023.
- [36] Y. Chen, Z. Wang, Y. Peng, Z. Zhang, G. Yu, and J. Sun, "Cascaded pyramid network for multi-person pose estimation," in *IEEE/CVF Conference on Computer Vision and Pattern Recognition (CVPR)*, 2018, pp. 7103–7112.
- [37] D. Rezende and S. Mohamed, "Variational inference with normalizing flows," in *International Conference on Machine Learning (ICML)*. PMLR, 2015, pp. 1530–1538.
- [38] R. Hartley and A. Zisserman, *Multiple view geometry in computer vision*, 2nd ed. Cambridge University Press, 2004.
- [39] M.-H. Guo, J.-X. Cai, Z.-N. Liu, T.-J. Mu, R. R. Martin, and S.-M. Hu, "Pct: Point cloud transformer," *Computational Visual Media*, vol. 7, pp. 187–199, 2021.
- [40] J. Ren, L. Pan, and Z. Liu, "Benchmarking and analyzing point cloud classification under corruptions," in *International Conference on Machine Learning (ICML)*. PMLR, 2022, pp. 18 559–18 575.
- [41] A. Vaswani, N. Shazeer, N. Parmar, J. Uszkoreit, L. Jones, A. N. Gomez, L. Kaiser, and I. Polosukhin, "Attention is all you need," *Advances in Neural Information Processing Systems (NeurIPS)*, vol. 30, 2017.
- [42] D. C. Liu and J. Nocedal, "On the limited memory bfgs method for large scale optimization," *Mathematical Programming*, vol. 45, no. 1-3, pp. 503–528, 1989.
- [43] M. Loper, N. Mahmood, J. Romero, G. Pons-Moll, and M. J. Black, "Smpl: A skinned multi-person linear model," *ACM Transactions on Graphics*, vol. 34, no. 6, pp. 1–16, 2015.
- [44] G. Moon, H. Choi, and K. M. Lee, "Neuralannot: Neural annotator for 3d human mesh training sets," in *IEEE/CVF Conference on Computer Vision and Pattern Recognition (CVPR)*, 2022, pp. 2299–2307.
- [45] G. Pavlakos, V. Choutas, N. Ghorbani, T. Bolkart, A. A. Osman, D. Tzionas, and M. J. Black, "Expressive body capture: 3d hands, face, and body from a single image," in *IEEE/CVF Conference on Computer Vision and Pattern Recognition (CVPR)*, 2019, pp. 10 975–10 985.
- [46] V. Davoodnia, S. Ghorbani, A. Messier, and A. Etemad, "Skelformer: Markerless 3d pose and shape estimation using skeletal transformers," *arXiv preprint arXiv:2404.12625*, 2024.
- [47] H. Joo, H. Liu, L. Tan, L. Gui, B. Nabbe, I. Matthews, T. Kanade, S. Nobuhara, and Y. Sheikh, "Panoptic studio: A massively multiview system for social motion capture," in *IEEE/CVF International Conference on Computer Vision (ICCV)*, 2015, pp. 3334–3342.
- [48] D. Remppe, T. Birdal, A. Hertzmann, J. Yang, S. Sridhar, and L. J. Guibas, "Humor: 3d human motion model for robust pose estimation," in *IEEE/CVF International Conference on Computer Vision (ICCV)*, 2021, pp. 11 488–11 499.
- [49] Z. Li, J. Liu, Z. Zhang, S. Xu, and Y. Yan, "Cliff: Carrying location information in full frames into human pose and shape estimation," in *European Conference on Computer Vision (ECCV)*. Springer, 2022, pp. 590–606.
- [50] M. Kocabas, C.-H. P. Huang, O. Hilliges, and M. J. Black, "Pare: Part attention regressor for 3d human body estimation," in *IEEE/CVF International Conference on Computer Vision (ICCV)*, 2021, pp. 11 127–11 137.
- [51] N. Kolotouros, G. Pavlakos, M. J. Black, and K. Daniilidis, "Learning to reconstruct 3d human pose and shape via model-fitting in the loop," in *IEEE/CVF International Conference on Computer Vision (ICCV)*, 2019, pp. 2252–2261.
- [52] S. Tripathi, L. Müller, C.-H. P. Huang, O. Taheri, M. J. Black, and D. Tzionas, "3d human pose estimation via intuitive physics," in *IEEE/CVF Conference on Computer Vision and Pattern Recognition (CVPR)*, 2023, pp. 4713–4725.
- [53] Z. Shen, Z. Cen, S. Peng, Q. Shuai, H. Bao, and X. Zhou, "Learning human mesh recovery in 3d scenes," in *IEEE/CVF Conference on Computer Vision and Pattern Recognition (CVPR)*, 2023, pp. 17 038–17 047.
- [54] A. Paszke, S. Gross, F. Massa, A. Lerer, J. Bradbury, G. Chanan, T. Killeen, Z. Lin, N. Gimelshein, L. Antiga *et al.*, "Pytorch: An imperative style, high-performance deep learning library," *Advances in Neural Information Processing Systems (NeurIPS)*, vol. 32, 2019.
- [55] M. Contributors, "Openmmlab pose estimation toolbox and benchmark," <https://github.com/open-mmlab/mmpose>, 2020.
- [56] K. He, X. Zhang, S. Ren, and J. Sun, "Deep residual learning for image recognition," in *IEEE/CVF Conference on Computer Vision and Pattern Recognition (CVPR)*, 2016, pp. 770–778.
- [57] M. Andriluka, L. Pishchulin, P. Gehler, and B. Schiele, "2d human pose estimation: New benchmark and state of the art analysis," in *IEEE/CVF Conference on Computer Vision and Pattern Recognition (CVPR)*, 2014, pp. 3686–3693.
- [58] I. Loshchilov and F. Hutter, "Decoupled weight decay regularization," in *International Conference on Learning Representations (ICLR)*, 2018.
- [59] X. Gong, L. Song, M. Zheng, B. Planche, T. Chen, J. Yuan, D. Doermann, and Z. Wu, "Progressive multi-view human mesh recovery with self-supervision," in *Proceedings of the AAAI Conference on Artificial Intelligence*, vol. 37, no. 1, 2023, pp. 676–684.
- [60] E. Remelli, S. Han, S. Honari, P. Fua, and R. Wang, "Lightweight multi-view 3d pose estimation through camera-disentangled representation," in *IEEE/CVF Conference on Computer Vision and Pattern Recognition (CVPR)*, 2020, pp. 6040–6049.
- [61] B. Gordon, S. Raab, G. Azov, R. Giryes, and D. Cohen-Or, "Flex: Extrinsic parameters-free multi-view 3d human motion reconstruction," in *European Conference on Computer Vision (ECCV)*. Springer, 2022, pp. 176–196.
- [62] B. Jiang, L. Hu, and S. Xia, "Probabilistic triangulation for uncalibrated multi-view 3d human pose estimation," in *IEEE/CVF International Conference on Computer Vision (ICCV)*, 2023, pp. 14 850–14 860.
- [63] P. Karashchuk, K. L. Rupp, E. S. Dickinson, S. Walling-Bell, E. Sanders, E. Azim, B. W. Brunton, and J. C. Tuthill, "Anipose: a toolkit for robust markerless 3d pose estimation," *Cell Reports*, vol. 36, no. 13, 2021.
- [64] A. Kendall, M. Grimes, and R. Cipolla, "Posenet: A convolutional network for real-time 6-dof camera relocalization," in *IEEE/CVF International Conference on Computer Vision (ICCV)*, 2015, pp. 2938–2946.
- [65] H. Rhodin, J. Spörri, I. Katircioglu, V. Constantin, F. Meyer, E. Müller, M. Salzmann, and P. Fua, "Learning monocular 3d human pose estimation from multi-view images," in *IEEE/CVF Conference on Computer Vision and Pattern Recognition (CVPR)*, 2018, pp. 8437–8446.
- [66] B. Wandt, M. Rudolph, P. Zell, H. Rhodin, and B. Rosenhahn, "Canonpose: Self-supervised monocular 3d human pose estimation in the wild," in *IEEE/CVF Conference on Computer Vision and Pattern Recognition (CVPR)*, 2021, pp. 13 294–13 304.
- [67] J. J. Sun, L. Karashchuk, A. Dravid, S. Ryou, S. Fereidooni, J. C. Tuthill, A. Katsaggelos, B. W. Brunton, G. Gkioxari, A. Kennedy *et al.*, "Bkind-3d: self-supervised 3d keypoint discovery from multi-view videos," in *IEEE/CVF Conference on Computer Vision and Pattern Recognition (CVPR)*, 2023, pp. 9001–9010.